JCTC Journal of Chemical Theory and Computation

Article

pubs.acs.org/JCTC

Molecular Models of Nanodiscs

Iwona Siuda and D. Peter Tieleman*

Department of Biological Sciences and Centre for Molecular Simulation, University of Calgary, 2500 University Drive North West, Calgary, Alberta T2N 1N4, Canada

Supporting Information

ABSTRACT: Nanodiscs are discoloidal protein−lipid particles that self-assemble from a mixture of lipids and membrane scaffold proteins. They form a highly soluble membrane mimetic that closely resembles a native-like lipid environment, unlike micelles. Nanodiscs are widely used for experimental studies of membrane proteins. In this work, we present a new method for building arbitrary nanodiscs using a combination of the Martini coarse-grained and all-atom force fields. We model the basic membrane scaffold protein MSP1 and its extended versions, such as MSP1E1 and MSP1E2, using a crystal structure of human apolipoprotein Apo-I. We test our method by generating nanodiscs of different sizes and compositions, including nanodiscs with embedded membrane proteins, such as bacteriorhodopsin, outer membrane protein X, and the glucose transporter. We show that properties of our nanodiscs are in general agreement with experimental data and previous computational studies.

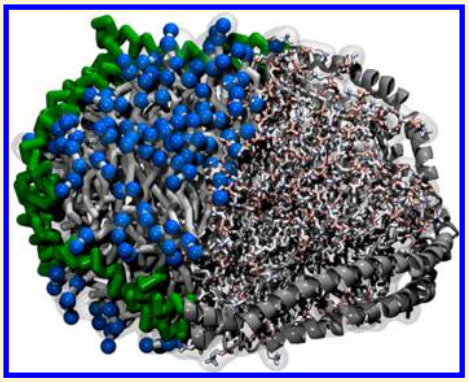

INTRODUCTION

Nanodiscs are discoloidal protein−lipid particles. They self-assemble from a detergent-solubilized mixture of lipids and membrane scaffold proteins (MSPs) upon slow removal of detergent.[1−6] During the self-assembly process, two copies of MSP wrap around a lipid bilayer patch, shielding the lipids' acyl chains from the aqueous environment and resulting in a soluble membrane mimetic.

The MSP is an engineered derivative of the binding domain of apolipoprotein A-I (ApoA-I).[1,2,7] ApoA-I itself is a 243-residue amphipathic protein divided into a 43-residue N-terminal globular domain followed by a 200-residue C-terminal lipid binding domain composed of two 11-residue and eight 22-residue helices punctuated by proline and glycine residues.[8] To date, three structures of human ApoA-I have been published, all in lipid-free states. These structures show more than 80% helical content.[9−11] The first structure is full-length ApoA-I (PDB: 2A01),[10] containing an N-terminal four-helix bundle and two shorter C-terminal helices. The other two structures are N-terminal truncations of ApoA-I. The first (PDB: 1AV1)[9] adopts a discoloidal shaped tetramer. The second one (PDB: 3R2P)[11] is a semicircle dimer. Because none of the ApoA-I structures has lipids bound, several models have been proposed for the arrangement of ApoA-I in nanodiscs, characterized by different conformations adopted by ApoA-I. These include the picket-fence model,[12] in which two ApoA-I are arranged on opposite sides of the nanodisc with the helices oriented parallel to the disc normal and the lipid acyl chains, and double-belt[13] and helical-hairpin[14] models, in which the ApoA-I helices are oriented perpendicular to the lipid acyl chains. In the double-belt model, two ApoA-I are wrapped around a lipid bilayer in head-to-tail fashion to form a belt. In the helical-hairpin model, two ApoA-I are on opposite sides of the nanodisc, each forming a single hairpin turn. Both experimental[15−19] and computational studies[4−6,20] strongly support the double-belt model for ApoA-I in nanodiscs.

Nanodiscs have attracted significant interest as a tool to study membrane proteins, resulting in a rapidly growing number of biophysical and biochemical studies of them. Their main advantage is that they provide a lipid bilayer-like environment in small soluble particles, unlike micelles, which are not bilayer-like, and vesicles, which are much larger. Other advantages include their stability, accessibility from both sides of the nanodisc, well-defined size and shape that can be modulated by truncation or repetition of the 11- and 22-residue stretches of the ApoA-I lipid binding domain,[1,21] and the possibility of controlling their lipid composition. The MSPs stabilize the lipid bilayer in solution and keep the inserted membrane protein in its oligomeric state, closely resembling a native-like lipid environment, ready for purification, manipulation, and structural and functional studies.[22,23] Nanodiscs have already been used as platform for studying a range of membrane proteins, including cytochrome P450s,[7,24] NADPH-cytochrome P450 reductase,[25] bacteriorhodopsin,[20,26,27] G-protein coupled receptors,[28,29] and outer membrane proteins A (OmpA)[30] and X (OmpX),[31] among others.

As there are no high-resolution structures of nanodiscs themselves, many studies have been dedicated to nanodisc self-assembly[1,4−6,21] and disassembly[32] processes, general characterization of nanodiscs[33,34] with a special interest in lipid behavior,[35,36] and the MSPs themselves.[1,4−6,13,20,21,37−42]

It this work, we present a new way of building molecular models of nanodiscs, where the size and composition are fully

Received: March 26, 2015
Published: September 2, 2015

DOI: 10.1021/acs.jctc.5b00668
J. Chem. Theory Comput. 2015, 11, 4923−4932

controlled, using computational methods. Our methods enables rapid creation of MSPs structures of different lengths, based on a template generated from a 200-residue lipid binding domain of ApoA-I, termed MSP1.[2] We also show how to generate extended constructs of MSP1, namely, MSP1E1 and MSP1E2 that have 22 and 44 additional amino acid residues, respectively. Next, we show how these structures can be used to build, in matter of minutes, an empty or a protein-loaded nanodisc that, after equilibration, can be used for molecular dynamic (MD) simulations. This is possible through the combination of coarse-grained (CG) and all-atom MD. We also show how to switch between the CG and all-atom models using the backward protocol.[43] The main interest of such simulations lies in the possibility of directly comparing experiments on proteins in nanodiscs with simulations and using the simulations to help interpret the experiments and to test assumptions about the properties of proteins and lipids in nanodiscs. They also demonstrate the importance of accurate experimental data that, in the absence of a high-resolution structure of the scaffold protein in an intact nanodisc, includes accurate numbers of lipids per nanodisc, the size and shape distribution of nanodiscs, and average lipid parameters, ideally, NMR order parameters.

METHODS

In this study, we used palmitoyloleoylphosphatidylcholine (POPC), dimyristoylphosphatidylcholine (DMPC), and monosialotetrahexosylganglioside (GM1) lipids and the crystal structures of Apo-A I,[9] bacteriorhodopsin (bR),[44] glucose transporter (GluT1),[45] and outer membrane protein X (OmpX).[46]We performed a set of molecular dynamics simulations using the GROMACS software package (ver. 4.5.7).[47,48] Each of the nanodisc systems consisted of two copies of an MSP, lipids, ions, and water molecules. When a protein-loaded disc was simulated, the system setup additionally included a crystal structure of a membrane protein. The initial distribution of the lipid and water molecules in the system was created using the bio.b-gen building tool.[49] A list of all simulations is given in Table S1, Supporting Information.

CG Simulation Parameters. The Martini CG model[50,51] for proteins[52,53] and the recently improved parameters for lipid molecules[54] were used in this study. The secondary and tertiary structures of the MSP and membrane proteins were maintained using the ElneDyn elastic network model[55] with the default force constant of F_c = 500 kJ mol^{-1} nm^{-2} and cut-offs r_{cutoff} = 0.7 nm for the MSPs and r_{cutoff} = 0.9 nm for the membrane proteins, if present in the system. The initial system was energy minimized (steepest descent, 1000 steps), neutralized with Na^+ counterions, and again energy minimized (steepest descent, 5000 steps). A three step equilibration was performed: (i) for 1 ns with initial time step of 10 fs, (ii) for 4 ns with a 20 fs time step and lipid molecules frozen in the z direction, (iii) for 5 ns with a 20 fs time step without any restraints. All subsequent simulations were run for 2 μs with a 20 fs time step, and the neighbor list was updated every 10 steps. The Lennard-Jones potential was shifted to zero between 0.9 and 1.2 nm, and the Coulomb potential was shifted to zero between 0 and 1.2 nm with a relative permittivity constant of ε_r = 15. An isotropic pressure coupling scheme of 1 bar was used for all simulations with a compressibility of 3 × 10^{-4} bar^{-1}. The pressure was relaxed in 5 ns simulation using the Berendsen barostat[56] with a relaxation time constant of τ_p = 5.0 ps; after that, a Parrinello–Rahman barostat[57] was used with τ_p = 12.0 ps. Temperature was kept at 310 K using the velocity rescaling thermostat[58] with a relaxation time constant of τ_T = 2.0 ps.

Backmapping to All-Atom Resolution. Conversion from Martini CG model to the Amber all-atom representation was done for nanodiscs and incorporated proteins only (no ion or water molecules included). A nanodisc was submitted to the backward protocol using the backward.py and initram.sh scripts.[43] All of the default settings remained unchanged except for the number of integration steps, which we increased from the default of 500 to 1000 for both the energy minimization with nonbonded interactions and the MD cycles. An additional step of distance-restrained simulation was run for 10 ps with a time step of 1 fs. The all-atom Amber99SB-ILDN force field[59] was used for proteins, and the Stockholm lipids (Slipids) force field[60−62] downloaded from Lipidbook[63] was used for lipids. The distance restraints were applied to the MSPs only, between the pairs of O (i) and H (i + 4) atoms, excluding the coil between helices 9 and 10, with a force constant of 5000 kJ mol^{-1} nm^{-2} with distance lower and upper limits of 0.19 and 0.23 nm, respectively. At this step, lipid molecules were kept fixed using freeze groups in all directions.

All-Atom Simulations. After the distance restraint step, the now atomistic nanodisc structure was resolvated using the TIP3P water model[64] and neutralized with Na^+ counterions. The system was energy minimized (steepest descent, 1000 steps) and equilibrated with position restraints (1000 kJ mol^{-1} nm^{-2}) applied to MSPs (and a membrane protein, if present) for 0.2 ns using a 2 fs time step. The resulting system was simulated for 50 ns using a 2 fs time step, and the neighbor list was update every 10 steps. The all-atom Amber99SB-ILDN force field[59] for protein and Slipids force field[60−62] for lipids were used. Long-range electrostatic interactions beyond 1.0 nm were calculated using particle mesh Ewald,[65] and the van der Waals interactions were switched to zero at 1.0 nm. Isotropic pressure was maintained at 1 bar, with a compressibility of 3 × 10^{-4} bar^{-1}, using the Parrinello–Rahman barostat[57] with a relaxation time of τ_p = 4.0 ps. Temperature was kept at 310 K using the velocity rescaling thermostat[58] with a relaxation time of τ_T = 0,1 ps.

Analysis. The last 1 μs of each of the CG simulations of empty nanodiscs and the last 40 ns of all-atom simulations of the MSP1 nanodisc with embedded OmpX and 140 DMPC lipids, and the empty MSP1E1 nanodisc with 206 DMPC lipids was used for the analyses. A cutoff 0.7 nm was assumed to represent one layer of CG POPC or DMPC lipids. Each nanodisc was divided into three circular layers in the xy plane (where z is the direction of the membrane normal): layer 1 (L1) includes lipids at a distance from 0 to 1.4 nm from the MSPs, layer 2 (L2) includes lipids at a distance between 1.4 and 2.8 nm from the MSPs, and the core of the nanodisc includes lipids at a distance greater than 2.8 nm from the MSPs. For comparison reasons, the same layers were defined for the all-atom MSP1E1 nanodisc. Visualization of the nanodiscs was performed with the molecular visualization program VMD.[66] The size of the nanodiscs and area per lipid were calculated using TCL scripts in VMD. The size of the nanodiscs was calculated as an average maximum distance between the MSPs in the x and y directions and averaged over time. The area per lipid was calculated for the core of the nanodisc for two leaflets separately and then averaged over two leaflets in time. For the CG nanodiscs, the nanodisc thickness, density, and lipid ordering plots were calculated using the GROMACS tools g_thickness, g_mydensity, and g_ordercg,[67] respectively, and

DOI: 10.1021/acs.jctc.5b00668
J. Chem. Theory Comput. 2015, 11, 4923−4932

plotted using dispgrid.py.[67] The plots are drawn with x and y dimension of 16 nm, using 100 bins in the x and y directions. The nanodisc thickness was calculated as the average distance between the phosphate PO_4 beads in the two leaflets as a function of distance from protein, with grid sampling with a spacing of ∼0.1 nm, averaged over time.[67] These values were then block averaged for the nanodisc layers (L2, L1, and core) and with calculated standard errors reported in Table 1. Similarly, a second-rank lipid order parameter, defined as

$$S = 1/2\langle 3\cos^2\theta - 1\rangle$$

where θ is the angle between the bond vector and the nanodisc normal, was calculated for all bonds in the lipid acyl chains as a function of distance from the protein with a grid sampling spacing of ∼0.2 nm and averaged within each bin (of 0.2 nm × 0.2 nm × 0.2 nm) over all bonds over time.[67] These order parameters were block averaged for the nanodisc layers (L2, L1, and core) and with calculated standard errors reported in Table 1. Nanodisc density was calculated as the average mass of the beads in the bin divided by the volume of the bin and averaged over time.

For the atomistic nanodisc, the nanodisc thickness was calculated as the distance between the centers of mass of phosphate atoms in two leaflets for each of the three layers of the nanodisc and averaged over time using the GROMACS g_dist tool. Deuterium order parameters were calculated for each lipid tail separately for each of the nanodisc layers and averaged over time using the GROMACS g_order tool. The atomistic and coarse-grained order parameters are not directly comparable, as they measure different orientations. The atomistic order parameters are related to the angle between the C−H bonds in the acyl chains and the normal on the disc, whereas the coarse-grained order parameters measure the orientation of the bond between two CG beads. The size of the nanodisc and area per lipid were calculated using TCL scripts in VMD, as described above.

RESULTS AND DISCUSSION

Our general approach is to create nanodiscs using the CG Martini model first. The much lower computational cost and the reduced complexity of the interaction potential combined make setup and equilibrium much easier than those with a fully atomistic setup. With the robust backward approach,[43] it is simple to create atomistic versions of the Martini models for atomistic simulations. We suggest that this is advantageous even if the Martini level itself is not of interest for a particular problem but is used only to create the models. Here, we describe the creation and analysis of both the atomistic and CG models.

It should be kept in the mind that there is no reliable experimental structure of the scaffold proteins in their actual nanodisc state. This means that even for a given model there is flexibility in the length of the scaffold simply by unfolding residues or by deforming helices. Simulations will have to incorporate assumptions about the structure of the scaffold proteins, regardless of the level of detail. In atomistic simulations, it is not possible to sample from an incorrect starting model to a correct structure, even if the force fields are accurate, whereas in Martini, the internal dynamics of proteins is not accurately represented and therefore requires assumptions about, at the very least, secondary structure. Essentially, there are three different parameters: the structure of the scaffold protein, the amount of lipids, and the packing of the lipids. If two are of them known, then simulations can predict the third with reasonable accuracy. The amount of lipids is usually the best-known quantity, although it would be of great interest to have more data on the other two.

Generating MSPs' Molecular Models of Different Lengths. The size and shape of the nanodisc are determined by two copies of MSPs that wrap around the phospholipid bilayer in a molecular double belt-like model.[13,15,68] The structure of human apolipoprotein A-I (Apo-I)[9] was previously optimized and used to engineer MSP of different lengths.[2] In this work, we are using chains A and B of the Apo-I crystal structure (PDB: 1AV1)[9] to model MSP1, MSP1E1, and MSP1E2. We start by coarse-graining Apo-I and applying the ElneDyn elastic network model with a force constant of F_c = 5000 kJ mol^{-1} nm^{-2} and cutoff value of r_{cutoff} = 1.2 nm to its backbone in its initial twisted conformation (Figure 1A). The high force constant and cutoff values for ElneDyn during the reshaping simulations serve to lock the specific interactions between two chains of Apo-I to those seen in the crystal structure.[9] We defined additional long (11.0 nm) elastic bonds between the backbone beads at the other ends of Apo-I structure, which helps to reshape the Apo-I structure into a circle (Figure 1B). This is a choice, as there is no experimental structure of the scaffold proteins in an actual nanodisc. The most detailed experimental studies suggest disc shapes and a narrow size distribution,[1,35] although this may depend on the conditions employed.[83] These elastic bonds are later removed, and the values for the elastic scaffold are reduced to more typical values of F_c = 500 kJ mol^{-1} nm^{-2} and r_{cutoff} = 0.7 nm to allow more realistic dynamics of the MSPs during the simulations.[55] Additionally, during the simulations, each of the MSPs is allowed to move independently of each other, as the elastic network is applied on each MSP individually (although other choices are, of course, possible).

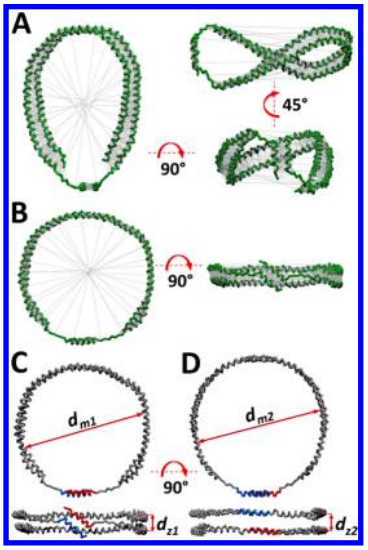

Figure 1. Reshaping the twisted conformation of apo A-I (A) into the ring structure of MSP1 (B) using the ElneDyn elastic network. Protein backbone beads are shown in green licorice representation. Elastic bonds are shown in gray. The backbones of MSP1 model 1 (C) and MSP1 model 2 (D) are shown in gray licorice. The C-terminal helices are marked in blue and red for chains A and B, respectively.

DOI: 10.1021/acs.jctc.5b00668
J. Chem. Theory Comput. 2015, 11, 4923−4932

Two models of MSP1 were created: **MSP1 m. 1** (Figure 1C) and **MSP1 m. 2** (Figure 1D), where m. stands for model. In **MSP1 m. 1**, the C-terminal helices from both chains are paired with each other and tilted ∼45° with respect to the *xy* plane of **MSP1 m. 1**. In the second model, the C-terminal helices are in the same plane as that in MSP1 and in the same planes as the chains of which they are a part. **MSP1 m. 1** has a diameter of d_{m1} = 11.0 nm, and the distance between two MSPs, excluding the C-termini helices, is, on average, d_{z1} = 1.9 nm. **MSP1 m. 2** is slightly larger, with a diameter of d_{m2} = 11.3 nm. and an average separation of two MSPs of d_{z2} = 2.2 nm along the entire circumference.

To engineer the extended constructs of MSP1,[69] MSP1 was again submitted to a reshaping simulation using ElneDyn. The resulting MSP1 chain is increased in diameter, with the gap between the N- and C-termini enlarged, yielding enough circumference to add additional helices to the original MSP1. By adding an additional 22 (helix 4 repeated) and 44 (helices 4 and 5 repeated) amino acid residues, we engineered MSP1E1 and MSP1E2, respectively. The amino acid sequences of MSP1, MSP1E1, and MSP1E2 can be found in the Supporting Information.

Building a Nanodisc. With the MSP coordinates in hand, we can now start building a nanodisc (Figure 2). If a protein-loaded nanodisc is built, then a protein of choice is positioned in the center of the MSPs (Figure 2B) or in another preferred position, e.g., above the center of the MSPs (Figure 2C). The initial reshaping of the MSPs makes it easy to scatter lipid molecules within the MSPs or around a membrane protein, if it is present in the system, within the MSPs. The lipid as well as water molecules is added to the system with the bio.b-gen tool. Next, the steric clashes are removed using bio.b-gen, and the resulting initial structure of the nanodisc is simulated using the standard procedure for CG MD simulations, i.e., the system is neutralized, energy minimized, and equilibrated. The example scripts for building an empty nanodisc can be found in Supporting Information.

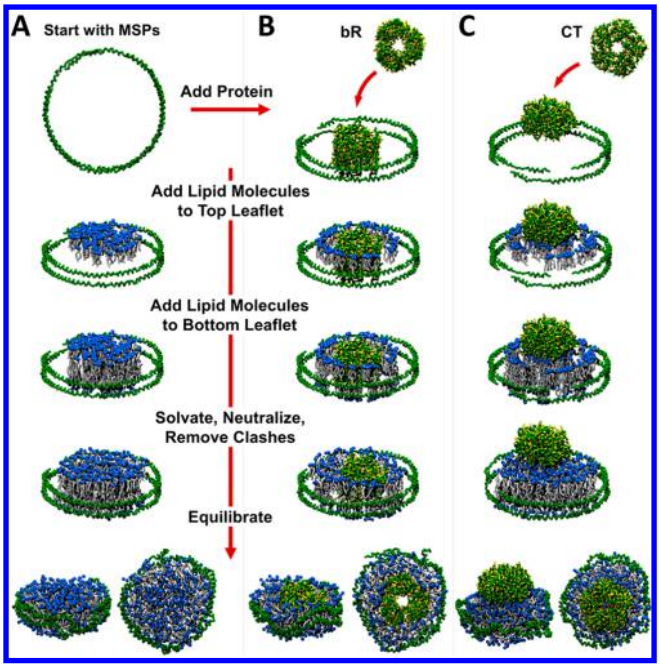

Figure 2. Diagram showing the steps in the process of building (A) an empty and (B, C) loaded nanodisc system. The proteins are shown in licorice representation. The backbone beads of MSPs, bR, and cholera toxin (CT) are shown in green; the side-chain beads of bR and CT are shown in yellow. The tails of DMPC lipid molecules are shown in gray licorice, and the phosphate and nitrogen beads are shown as blue spheres. Ions and water molecules have been omitted for clarity.

To test the method, we built 36 different empty or protein-loaded nanodiscs, and we simulated them for 2 μs each. The number of lipids for different nanodiscs was estimated based on previously reported experimental and computational data and was used as an input parameter for the method. The number of POPC and DMPC lipids for MSP1 was chosen to be between 112 and 166 lipids based on numbers estimated by gel filtration chromatography,[26] scintillation counting of tritiated lipids,[1] and reported in a previous MD study.[12] The number of DMPC lipids for empty MSP1E1 and MSP1E2 nanodiscs ranged between 186 and 250 and was based on gel filtration chromatography done on a set of self-assembled nanodiscs with the same type of MSPs but a different number of DMPC lipids.[26] The same study was used to determine the number of DMPC lipids for bR trimer-loaded MSP1E1 and MSP1E2 nanodiscs, where it has been shown that bR displaces, on average, 30−40 molecules of DMPC per bR monomer. Therefore, for bR trimer-loaded MSP1E1 nanodiscs, we tested 110 and 120 DMPC lipids, whereas for bR trimer-loaded MSP1E2 nanodiscs, we tested 120 and 130 DMPC lipids. GluT1-loaded MSP1E1 nanodisc with 186 DMPC lipids and MSP1E1 nanodiscs with GM1:DMPC ratios of 18:168, 20:186, and 22:204 were built based on an educated guess. The OmpX-loaded MSP1 nanodisc was built with 140 DMPC lipids using an NMR study of OmpA as a reference.[30] A list of all simulations is given in Table S1, Supporting Information.

The nanodiscs maintained their initial discoloidal shape (Figure 3) with minimal distortion throughout the length of the simulations. The same observation was previously reported for self-assembled CG nanodiscs during 1 μs.[4] This stability is expected at the simulated temperature of 310 K because, experimentally, nanodiscs were shown to be stable up to 330 K, at which point irreversible aggregation of the nanodiscs occurs.[35]

Our method proved to be successful in building not only empty nanodiscs with one type of lipids, or a mixture of lipids where the ratio of the lipids is fully controlled, but also protein-loaded nanodiscs. Several previous computational studies used self-assembly to build nanodiscs.[5,6,20] This was proposed mainly to gain insights into the self-assembly process itself[3,26,27,69] However, even though the self-assembly process has been studied extensively by CG MD simulations,[4,5,70−73] the resulting nanodiscs composition will always be somewhat uncontrolled, as the final structures are, in part, determined by metastable intermediates during the assembly process. For simulations of practical applications, a more systematic way to build nanodiscs is preferable and is considerably cheaper computationally.

Building protein-loaded nanodiscs using our method is straightforward compared to that using an atomistic protocol[20] in which a protein-loaded nanodisc is built by first building and equilibrating an empty nanodisc from which lipids are then removed to form a hole for inserting a membrane protein. Although this method works, in analogy with existing methods to insert atomistic membrane proteins in lipid bilayers, it is more difficult to automate, and equilibration of the perturbed lipids around the protein is time-consuming, especially for lipid mixtures. A similar protocol using Martini as an intermediate

DOI: 10.1021/acs.jctc.5b00668
J. Chem. Theory Comput. 2015, 11, 4923−4932

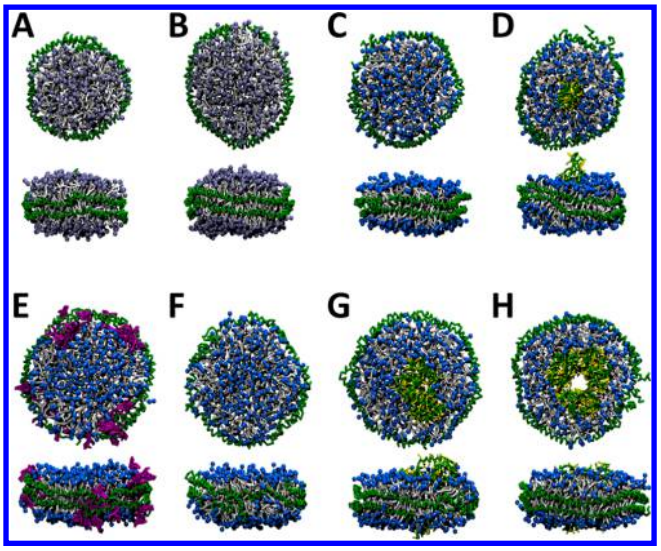

Figure 3. Example structures from the simulations of nanodiscs built with (A) MSP1 and 122 POPC lipids, (B) MSP1 and 160 POPC lipids, (C) MSP1 and 162 DMPC lipids, (D) MSP1, OmpX, and 140 DMPC lipids, (E) MSP1E1, 22 GM1 glycolipids, and 204 DMPC lipids, (F) MSP1E1 and 206 DMPC lipids, (G) MSP1E1, GluT1, and 186 DMPC lipids, and (H) MSP1E2, bR trimer, and 130 DMPC lipids. The MSPs and DMPC are colored as described in Figure 2. The POPC tails are colored the same as DMPC lipids tails, and the phosphate and nitrogen beads are shown as vdW spheres, in ice blue for POPC and blue for DMPC. The GM1 glycolipids are shown in magenta licorice. The backbone beads of OmpX, GluT1, and bR are shown in green, and the side chain beads are shown in yellow.

would give comparable results with a similar amount of effort to what we propose here.

Nanodisc Properties. From the 26 simulations of empty nanodiscs, we excluded the simulations that included nanodiscs built with **MSP1 m. 2** because the results in terms of lipid properties (data not shown) were similar to the output from simulations using **MSP1 m. 1**. For the remaining set of 16 simulations with either DMPC or POPC lipids, we measured the size of the nanodisc and calculated the area per lipid for the nanodisc core. We also calculated the thickness and the lipid order parameter for three different areas: L2, L1, and core of the nanodisc. Table 1 shows the results for **MSP1 m. 1** (MSP1) and results for MSP1E1 and MSP1E2 nanodiscs.

The size of the nanodisc depends not only on the length of the MSPs used but also on the number of lipids that were given as an input parameter to the method. For the MSP1 nanodiscs, the size is calculated to be between 8.9 ± 0.3 and 10.7 ± 1.0 nm, for MSP1E1, between 10.4 ± 0.6 and 11.4 ± 0.0 nm, and for MSP1E2, between 11.6 ± 0.7 and 12.0 ± 0.7 nm, depending on the number of lipids. Our results are in general agreement with previously reported nanodiscs diameters determined by size exclusion chromatography (SEC)[1,26] and small-angle X-ray scattering (SAXS),[1] which was reported to be between 9.1 and 9.8 nm for MSP1, 10.0 and 10.6 nm for MSP1E1, and 10.7 and 11.9 nm for MSP1E2.

We observed that the nanodisc thickness increases with increasing distance from the MSPs. These observations are consistent with previously reported all-atom[20] and CG nanodisc simulations[4] as well as SASX measurements,[1,35] which revealed similar changes in the nanodisc thickness and perturbation of boundary lipids. The perturbation of boundary lipids can be explained by the distorted packing of the lipids at the protein−lipid interface, as the boundary lipids adjust to the protein surface to minimize hydrophobic mismatch. The boundary lipids, therefore, are expected to have a larger area per lipid and thus smaller bilayer height. The calculated thickness from our simulations in L2 is between 3.0 ± 0.3 and 3.4 ± 0.5 nm for MSP1, 2.8 ± 0.3 and 3.3 ± 0.3 nm for MSP1E1, and 2.7 ± 0.3 and 2.9 ± 0.3 nm for MSP1E2.

We observe that the thickness of the core area of the nanodiscs with POPC lipids is between 4.3 ± 0.0 and 4.4 ± 0.0 nm, whereas for nanodiscs with DMPC lipids, the thickness is lower, as expected, between 3.5 ± 0.0 and 3.6 ± 0.0 nm. The difference of ∼0.8 nm is to be expected from the difference in the length of lipids' acyl chains, C_{16}/C_{18} versus C_{14}.

Table 1. Nanodisc Properties

					thickness (nm)			order parameter *S*		
MSP	no. l.[a]	lipid type	size (nm)	APL[b] (nm^2)	core[c]	L1[d]	L2[e]	core[c]	L1[d]	L2[e]
MSP1	112	POPC	9.18 ± 1.12	0.82 ± 0.09	4.32 ± 0.02	4.25 ± 0.08	3.39 ± 0.46	0.36 ± 0.01	0.25 ± 0.05	0.13 ± 0.04
MSP1	122	POPC	8.85 ± 0.27	0.73 ± 0.10	4.35 ± 0.01	4.24 ± 0.09	3.43 ± 0.37	0.35 ± 0.01	0.23 ± 0.05	0.11 ± 0.07
MSP1	132	POPC	9.21 ± 0.41	0.71 ± 0.02	4.33 ± 0.02	4.21 ± 0.10	3.35 ± 0.39	0.35 ± 0.01	0.23 ± 0.05	0.10 ± 0.07
MSP1	160	POPC	10.29 ± 0.33	0.71 ± 0.04	4.27 ± 0.02	4.22 ± 0.08	3.46 ± 0.38	0.34 ± 0.01	0.21 ± 0.04	0.07 ± 0.08
MSP1	150	DMPC	9.49 ± 0.13	0.65 ± 0.05	3.59 ± 0.02	3.60 ± 0.04	2.99 ± 0.34	0.38 ± 0.004	0.30 ± 0.05	0.15 ± 0.07
MSP1	154	DMPC	9.62 ± 0.10	0.64 ± 0.03	3.64 ± 0.02	3.59 ± 0.06	2.99 ± 0.26	0.38 ± 0.003	0.31 ± 0.05	0.14 ± 0.08
MSP1	158	DMPC	10.19 ± 0.73	0.62 ± 0.04	3.62 ± 0.02	3.60 ± 0.05	3.01 ± 0.28	0.37 ± 0.004	0.29 ± 0.05	0.12 ± 0.09
MSP1	162	DMPC	10.22 ± 0.16	0.64 ± 0.06	3.58 ± 0.02	3.61 ± 0.3	3.03 ± 0.32	0.38 ± 0.003	0.30 ± 0.05	0.13 ± 0.08
MSP1	164	DMPC	10.18 ± 0.05	0.63 ± 0.01	3.59 ± 0.02	3.61 ± 0.04	3.06 ± 0.30	0.38 ± 0.003	0.31 ± 0.05	0.14 ± 0.08
MSP1	166	DMPC	10.65 ± 1.04	0.67 ± 0.01	3.56 ± 0.02	3.57 ± 0.03	3.02 ± 0.30	0.38 ± 0.002	0.31 ± 0.05	0.14 ± 0.08
MSP1E1	186	DMPC	10.35 ± 0.59	0.62 ± 0.06	3.58 ± 0.02	3.57 ± 0.07	2.85 ± 0.35	0.37 ± 0.01	0.29 ± 0.06	0.10 ± 0.08
MSP1E1	206	DMPC	11.00 ± 0.06	0.62 ± 0.02	3.57 ± 0.03	3.56 ± 0.07	2.78 ± 0.39	0.38 ± 0.004	0.29 ± 0.06	0.10 ± 0.07
MSP1E1	226	DMPC	11.42 ± 0.03	0.60 ± 0.01	3.52 ± 0.03	3.55 ± 0.05	2.96 ± 0.31	0.37 ± 0.01	0.29 ± 0.06	0.10 ± 0.08
MSP1E2	238	DMPC	11.57 ± 0.67	0.64 ± 0.06	3.57 ± 0.03	3.54 ± 0.08	2.89 ± 0.26	0.36 ± 0.01	0.29 ± 0.06	0.10 ± 0.08
MSP1E2	244	DMPC	11.69 ± 0.23	0.65 ± 0.01	3.49 ± 0.03	3.44 ± 0.10	2.75 ± 0.28	0.36 ± 0.01	0.27 ± 0.06	0.08 ± 0.08
MSP1E2	250	DMPC	11.97 ± 0.66	0.66 ± 0.03	3.55 ± 0.03	3.54 ± 0.08	2.84 ± 0.31	0.36 ± 0.01	0.28 ± 0.06	0.09 ± 0.08

[a]No. l., number of lipids. [b]APL, area per lipid. [c]Core, lipids at the distance >2.8 nm from MSP. [d]L1, layer 1, lipids between 1.4 and 2.8 nm from MSP. [e]L2, layer 2, lipids between 0 and 1.4 nm from MSP.

DOI: 10.1021/acs.jctc.5b00668
J. Chem. Theory Comput. 2015, 11, 4923−4932

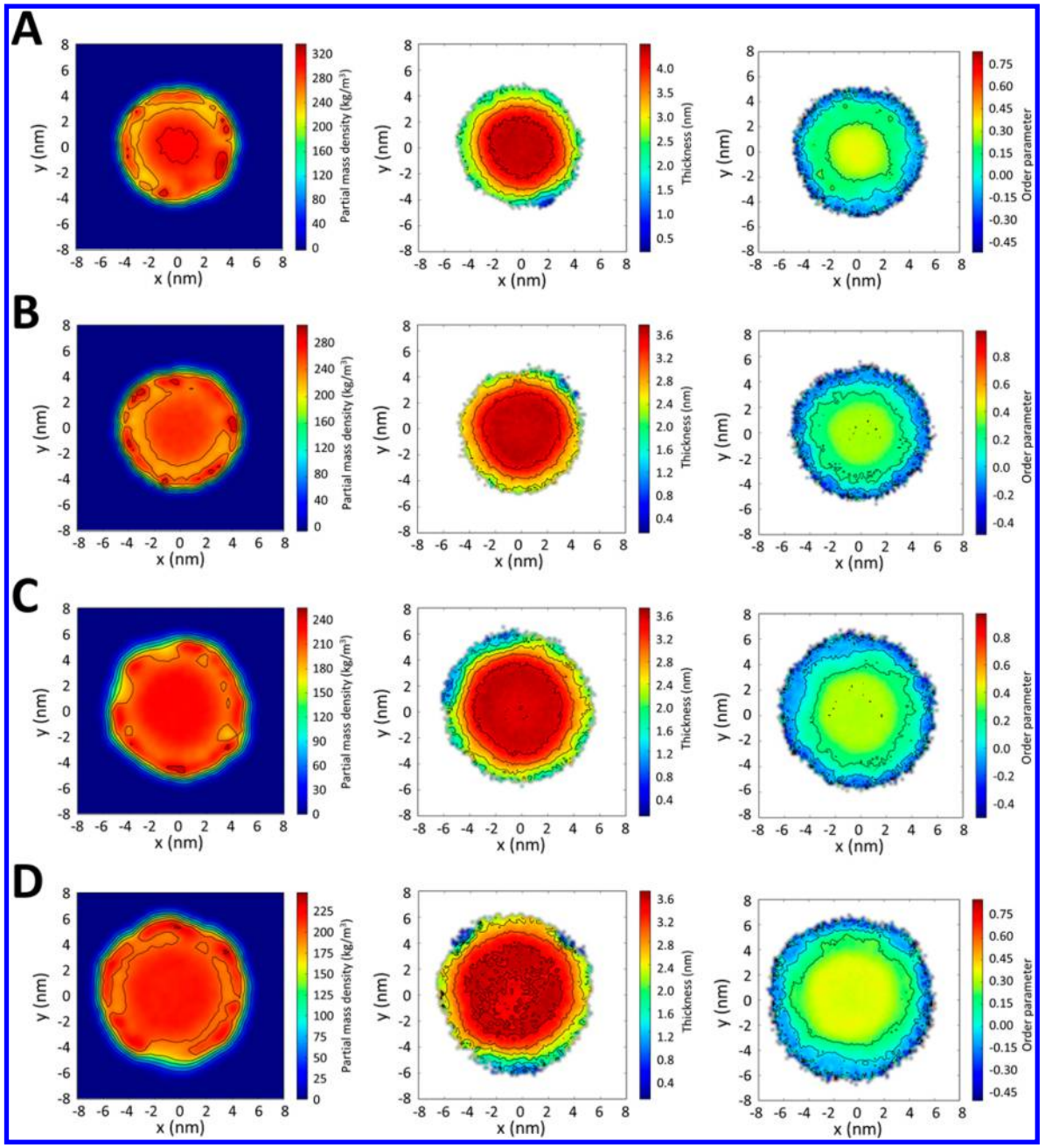

Figure 4. Membrane density (left panels), membrane thickness (central panels), and lipid acyl chain order parameter (right panels) for nanodiscs: (A) MSP1 and 132 POPC lipids, (B) MSP1 and 154 DMPC lipids, (C) MSP1E1 and 206 DMPC lipids, and (D) MSP1E2 and 244 DMPC lipids.

The area per lipid, for the same reasons as explained in the previous paragraph, decreases with the distance from the MSPs and is dependent on the lipid type. For smaller nanodiscs containing fewer lipids, the area per lipid is expected to be higher than for larger nanodiscs built with the same MSPs, as the fraction of structurally perturbed boundary lipids is significantly higher in smaller nanodiscs. In our simulations, the nanodiscs with POPC lipids have a core area per lipid in the range of 0.7−0.8 nm^2, which is comparable with a previously estimated area per lipid of 0.7 nm for POPC averaged over the whole nanodisc.[1] The nanodiscs with DMPC lipids have a core area per lipid between 0.6 and 0.7 nm^2. This difference for POPC and DMPC lipids also can be attributed to general properties of lipids, where an experimental estimate of the area per lipid for fully hydrated POPC bilayer is 0.64 ± 0.01 nm^2[74] and is slightly higher than 0.61 ± 0.01 nm^2, which is an experimental estimate for fully hydrated DMPC.[75,76]

The order parameter S that describes the average ordering of the lipid chains also varies depending on the distance from MSPs (Table 1). A similar pattern as for nanodisc thickness is observed, with the lipids' ordering increasing with the distance from the MSPs. As seen in Table 1, in layer L2, at the protein−lipid interface, lipids' tails are poorly aligned with the normal, whereas L1 is a type of buffer layer where lipids' tails shift into a more aligned distribution along the z axis. In general, the nanodiscs with POPC lipids are less ordered, with an average order parameter of 0.2 for the core of the nanodisc, than the nanodiscs with DMPC, for which the average lipid order parameter for the core is 0.3. This can be attributed to the fact that the core of the nanodiscs with POPC lipids has a smaller

DOI: 10.1021/acs.jctc.5b00668
J. Chem. Theory Comput. 2015, 11, 4923−4932

area compared to that of nanodiscs with DMPC lipids that are (in our case) generally larger and thus are more affected by the perturbation at the protein−lipid interface. Additionally, unsaturation increases lipid disorder;[77] therefore, POPC is expected to be more disordered than DMPC. Overall, the CG order parameters are similar to those observed in previous bilayer simulations with embedded peptides, which also calculated 2D maps across the system,[84] but specific values depend on lipid packing and thus on the assumptions embedded in the modeled structure of the scaffold protein and the number of lipids added.

The thickness and lipid order parameter plots (Figure 4) for MSP1 nanodiscs with POPC and DMPC and for MSP1E1 and MSP1E2 nanodiscs with DMPC lipids show a clear separation into layers. The density plots (Figure 4) show that the densities are more or less uniform with the exception of the area at the boundary between L2 and L1, where, due to the arrangement of lipids' tails, there are fewer lipids' head groups present.

Atomistic Simulations: Backmapping. For comparison to many experimental systems where atomistic details of specific membrane proteins are of interest, atomistic models are required. With the recently published backward protocol,[43] this is possible for complex systems, including lipid membranes,[78] model peptides,[79] and proteins.[80,81] During backmapping, the MSPs' secondary structure was poorly defined (Figure 5A); therefore, we added an additional step of distance restraints during which the MSPs' secondary structure was fixed (Figure 5B). This step allows us to obtain a well-defined nanodisc structure that can be used as the starting structure for all-atom simulations. During the equilibration process, the ideal helical structure of MSPs relaxes and follows the force field parametrization.

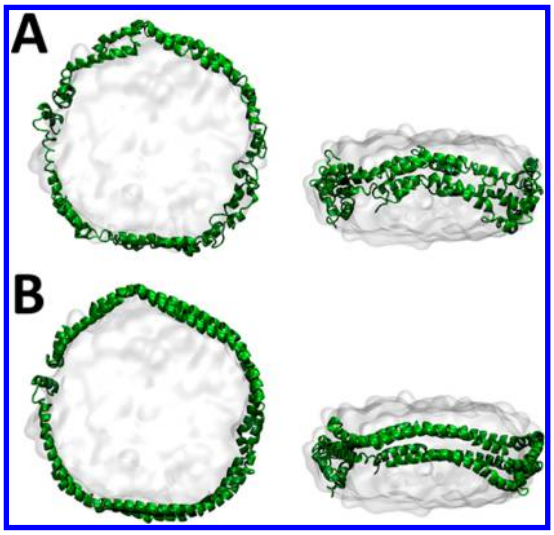

Figure 5. Empty nanodisc in all-atom representation (A) after backmapping and (B) after the distance restraint step. The MSPs are shown in NewCartoon representation in green. The DMPC lipid molecules are shown as a transparent surface.

We backmapped selected structures of the MSP1 nanodisc with OmpX and 140 DMPC lipids and the MSP1E1 nanodisc with 206 DMPC lipids back to atomistic resolution and compared them to corresponding CG nanodiscs in terms of nanodisc size, thickness, and lipid ordering using empty nanodics and in terms of protein behavior, as well as nanodisc size, using the protein-loaded nanodisc.

The size of each of atomistic nanodisc is 10.9 ± 0.3 nm in diameter for empty nanodiscs and 10.3 ± 0.2 nm for protein-loaded nanodiscs, essentially the same as the 11.0 ± 0.1 and 10.2 ± 0.3 nm for empty and protein-loaded CG nanodiscs, respectively. Similar to the thickness of the CG MSP1E1 empty nanodisc, the thickness of the atomistic nanodisc changes with the distance from the MSPs. The calculated values for three layers, L2 = 2.9 ± 0.0 nm, L1 = 3.7 ± 0.0 nm, and core = 3.7 ± 0.0 nm, are comparable with the thickness of the CG nanodisc, whereas the lipid ordering also shows that the lipids at the protein−lipid interface are less ordered, as is the case in the CG nanodisc; however, the values are more uniform than those for the CG nanodisc (Table 2). The values themselves are lower because they are deuterium S_{cd} order parameters and are generally comparable to experimental and simulation values for PC lipids, although the exact values, as in the CG case, depend on simulation assumptions: the structure of the scaffold protein and the number of lipids in the nanodisc for a given scaffold protein. The separation of lipid layers in nanodiscs is shown in Figure 6 for both all-atom and CG structures of the empty

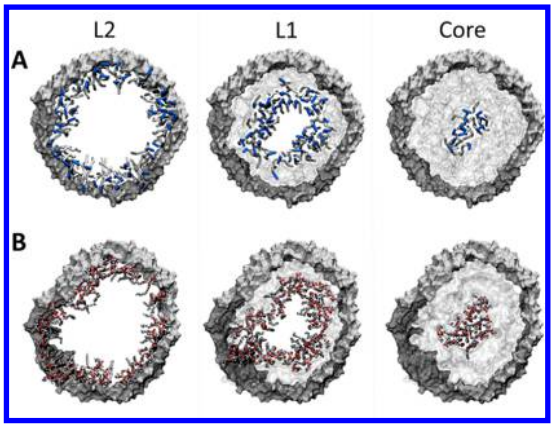

Figure 6. Empty nanodisc in (A) CG and (B) all-atom representations, showing lipids in different nanodisc layers (L2, L1, and core). The MSPs are shown in surface representation in gray. The CG DMPC lipid molecules are shown in licorice in white, with phosphate and nitrogen beads shown in blue, and the all-atom DMPC lipids are shown in licorice; the carbon, oxygen, phosphate, nitrogen atoms are shown in cyan, red, tan, and blue, respectively.

Table 2. All-Atom and CG MSP1E1 Nanodiscs Comparison

			thickness (nm)			order parameter S^a		
simulation type	size (nm)	APL[b] (nm^2)	core[c]	L1[d]	L2[e]	core[c]	L1[d]	L2[e]
all-atom	10.9 ± 0.3	0.66 ± 0.04	3.73 ± 0.04	3.66 ± 0.02	2.87 ± 0.03	0.17 ± 0.03	0.16 ± 0.01	0.14 ± 0.02
CG	11.0 ± 0.1	0.62 ± 0.02	3.57 ± 0.03	3.56 ± 0.07	2.78 ± 0.39	0.38 ± 0.01	0.29 ± 0.06	0.10 ± 0.07

[a]The order parameter for both tails is the same. [b]APL, area per lipid. [c]Core, lipids at the distance >2.8 nm from MSP. [d]L1, layer 1, lipids between 1.4 and 2.8 nm from MSP. [e]L2, layer 2, lipids between 0 and 1.4 nm from MSP.

DOI: 10.1021/acs.jctc.5b00668
J. Chem. Theory Comput. 2015, 11, 4923−4932

MSP1E1 nanodisc, for comparison. The area per lipid for the core layer for the all-atom nanodisc is 0.6 ± 0.0 and is in the same range as the area per lipid for nanodiscs with DMPC lipids (0.6−0.7 nm^2).

In addition to structural properties, the simulations give access to detailed dynamical properties in terms of lipid diffusion and, in principle, other more detailed properties. However, these are, to our knowledge, difficult to access experimentally. Because of the finite size of the nanodiscs, diffusion coefficients are defined only for a given time scale, as the long-term diffusion coefficient is zero because of the protein boundary. At very short time scales, they are also position-dependent, as lipids near the middle of the disc can be expected to behave differently from lipids at the edge. The mean square displacement vs time gives an idea of relative diffusion coefficients at short time scales for different lipids as well as for a comparison between atomistic and coarse-grained simulations. Figure S2 shows, basically, expected behavior. The maximum displacement depends on the size of the nanodisc. The initial slope of the mean square displacement vs time is several times higher for Martini simulations compared to that of atomistic simulations, consistent with the properties of Martini. The maximum MSD is highest for the DMPC nanodisc, which is significantly larger than the POPC nanodisc. In both atomistic and CG simulations, DMPC diffuses faster than POPC, with a much larger difference in Martini. We visually inspected the trajectories of all of the lipids in the CG nanodiscs, which readily diffuse throughout the disc regardless of initial position. Interactions with the scaffold protein, at least for these PC lipids, are only transient on a time scale of <100 ns.

To assess the changes in protein structure, we measured the RMSD of the final structures of MSP1, compared to the initial structure of the simulation, and OmpX, compared to the crystal structure, for both the all-atom and CG simulations. In the all-atom simulation, the MSP1 structure is stable with an RMSD of 0.2 nm, whereas in the CG simulation, the RMSD is higher at 0.7 nm. This difference is to be expected, as the ElneDyn network on MSP1 is too weak to accommodate the changes in the protein needed to adjust to the amount of lipids in the nanodisc, whereas in the all-atom simulation, this step is not present because the backmapped structure of the nanodisc is derived from a well-equilibrated CG structure, whereas the sampling time in the atomistic simulations is not enough for drastic rearrangements. The OmpX in both simulations is stable, with an RMSD of 0.2 nm for both cases. The OmpX structure in the atomistic simulation starts from essentially the crystal structure, which is used in the backmapping procedure, so 0.2 nm is after a 50 ns simulation. In the CG simulation, the structure is stabilized by an elastic network that has been parametrized to give similar RMSDs but can be modified, e.g., to incorporate separate networks for different domains.[82] Other changes in this network can be made to accommodate specific questions on specific protein systems.

CONCLUSIONS

We have proposed a new method for building molecular models of nanodiscs, where the size and composition of the system is fully controlled. We tested the method by building 36 different empty and protein-loaded nanodiscs. The overall structure and properties, such as thickness, lipid order parameter, and area per lipid, are in good agreement with previously reported experimental and computational studies, but experimental information or educated guesses are required to determine the number of lipids that should fill the nanodisc, as this can be determined only approximately by computation. The size of the nanodiscs depends on the length of the used MSPs and, for a given MSP, on the amount of lipids in the nanodisc. Taken together, these data show that our model is a good choice not only for studying the properties of the nanodiscs themselves but also for structural and functional studies of membrane proteins. With the possibility of reversing the CG structure into an all-atom model, one can focus on more detailed analyses.

ASSOCIATED CONTENT

Supporting Information

The Supporting Information is available free of charge on the ACS Publications website at DOI: 10.1021/acs.jctc.5b00668.

Set of final structures of nanodiscs: MSP1 with POPC and DMPC lipids, MSP1E1 with DMPC lipids and mixture of GM1:DMPC lipids, and MSP1E2 with bR trimer and DMPC lipids (ZIP).

Sequences of MSP1, MSP1E1, and MSP1E2 built in this study; list of all simulations; example scripts for building an empty nanodisc; nanodisc structures; mean square displacements (PDF).

AUTHOR INFORMATION

Corresponding Author

*E-mail: tieleman@ucalgary.ca.

Funding

This work was supported by the Natural Sciences and Engineering Research Council of Canada, grant RGPIN/238357. D.P.T. is an Alberta Innovates Health Solutions Scientist and Alberta Innovates Technology Futures Strategic Chair in (Bio)Molecular Simulation. Calculations were carried out on Compute Canada facilities.

Notes

The authors declare no competing financial interest.

ACKNOWLEDGMENTS

The authors would like to thank Dr. Dmitri Rozmanov for writing the bio.b-gen program.

REFERENCES

(1) Denisov, I. G.; Grinkova, Y. V.; Lazarides, a a; Sligar, S. G. Directed Self-Assembly of Monodisperse Phospholipid Bilayer Nanodiscs with Controlled Size. *J. Am. Chem. Soc.* **2004**, *126*, 3477−3487.

(2) Bayburt, T. H.; Grinkova, Y. V.; Sligar, S. G. Self-Assembly of Discoidal Phospholipid Bilayer Nanoparticles with Membrane Scaffold Proteins. *Nano Lett.* **2002**, *2*, 853−856.

(3) Bayburt, T. H.; Sligar, S. G. Membrane Protein Assembly into Nanodiscs. *FEBS Lett.* **2010**, *584*, 1721−1727.

(4) Shih, A. Y.; Arkhipov, A.; Freddolino, P. L.; Schulten, K. Coarse Grained Protein−Lipid Model with Application to Lipoprotein Particles†. *J. Phys. Chem. B* **2006**, *110*, 3674−3684.

(5) Shih, A. Y.; Freddolino, P. L.; Arkhipov, A.; Schulten, K. Assembly of Lipoprotein Particles Revealed by Coarse-Grained Molecular Dynamics Simulations. *J. Struct. Biol.* **2007**, *157*, 579−592.

(6) Shih, A. Y.; Arkhipov, A.; Freddolino, P. L.; Sligar, S. G.; Schulten, K. Assembly of Lipids and Proteins into Lipoprotein Particles. *J. Phys. Chem. B* **2007**, *111*, 11095−11104.

(7) Bayburt, T. H.; Carlson, J. W.; Sligar, S. G. Reconstitution and Imaging of a Membrane Protein in a Nanometer-Size Phospholipid Bilayer. *J. Struct. Biol.* **1998**, *123*, 37−44.

DOI: 10.1021/acs.jctc.5b00668
J. Chem. Theory Comput. 2015, 11, 4923−4932

(8) Boguski, M. S.; Freeman, M.; Elshourbagy, N. A.; Taylor, J. M.; Gordon, J. I. On Computer-Assisted Analysis of Biological Sequences: Proline Punctuation, Consensus Sequences, and Apolipoprotein Repeats. *J. Lipid Res.* **1986**, *27*, 1011−1034.
(9) Borhani, D. W.; Rogers, D. P.; Engler, J. A.; Brouillette, C. G. Crystal Structure of Truncated Human Apolipoprotein A-I Suggests a Lipid-Bound Conformation. *Proc. Natl. Acad. Sci. U. S. A.* **1997**, *94*, 12291−12296.
(10) Ajees, A. A.; Anantharamaiah, G. M.; Mishra, V. K.; Hussain, M. M.; Murthy, H. M. K. Crystal Structure of Human Apolipoprotein A-I: Insights into Its Protective Effect against Cardiovascular Diseases. *Proc. Natl. Acad. Sci. U. S. A.* **2006**, *103*, 2126−2131.
(11) Mei, X.; Atkinson, D. Crystal Structure of C-Terminal Truncated Apolipoprotein A-I Reveals the Assembly of High Density Lipoprotein (HDL) by Dimerization. *J. Biol. Chem.* **2011**, *286*, 38570−38582.
(12) Phillips, J. C.; Wriggers, W.; Li, Z.; Jonas, A.; Schulten, K. Predicting the Structure of Apolipoprotein A-I in Reconstituted High-Density Lipoprotein Disks. *Biophys. J.* **1997**, *73*, 2337−2346.
(13) Segrest, J. P.; Jones, M. K.; Klon, A. E.; Sheldahl, C. J.; Hellinger, M.; De Loof, H.; Harvey, S. C. A Detailed Molecular Belt Model for Apolipoprotein A-I in Discoidal High Density Lipoprotein. *J. Biol. Chem.* **1999**, *274*, 31755−31758.
(14) Brouillette, C. G.; Anantharamaiah, G. M. Structural Models of Human Apolipoprotein A-I. *Biochim. Biophys. Acta, Lipids Lipid Metab.* **1995**, *1256*, 103−129.
(15) Koppaka, V.; Silvestro, L.; Engler, J. A.; Brouillette, C. G.; Axelsen, P. H. The Structure of Human Lipoprotein A-I: EVIDENCE FOR THE "BELT" MODEL. *J. Biol. Chem.* **1999**, *274*, 14541−14544.
(16) Li, Y.; Kijac, A. Z.; Sligar, S. G.; Rienstra, C. M. Structural Analysis of Nanoscale Self-Assembled Discoidal Lipid Bilayers by Solid-State NMR Spectroscopy. *Biophys. J.* **2006**, *91*, 3819−3828.
(17) Davidson, W. S.; Hilliard, G. M. The Spatial Organization of Apolipoprotein A-I on the Edge of Discoidal High Density Lipoprotein Particles: A MASS SPECTROMETRY STUDY. *J. Biol. Chem.* **2003**, *278*, 27199−27207.
(18) Silva, R. A. G. D.; Hilliard, G. M.; Li, L.; Segrest, J. P.; Davidson, W. S. A Mass Spectrometric Determination of the Conformation of Dimeric Apolipoprotein A-I in Discoidal High Density Lipoproteins. *Biochemistry* **2005**, *44*, 8600−8607.
(19) Martin, D. D. O.; Budamagunta, M. S.; Ryan, R. O.; Voss, J. C.; Oda, M. N. Apolipoprotein A-I Assumes a "Looped Belt" Conformation on Reconstituted High Density Lipoprotein. *J. Biol. Chem.* **2006**, *281*, 20418−20426.
(20) Shih, A. Y.; Denisov, I. G.; Phillips, J. C.; Sligar, S. G.; Schulten, K. Molecular Dynamics Simulations of Discoidal Bilayers Assembled from Truncated Human Lipoproteins. *Biophys. J.* **2005**, *88*, 548−556.
(21) Grinkova, Y. V.; Denisov, I. G.; Sligar, S. G. Engineering Extended Membrane Scaffold Proteins for Self-Assembly of Soluble Nanoscale Lipid Bilayers. *Protein Eng., Des. Sel.* **2010**, *23*, 843−848.
(22) Bayburt, T. H.; Vishnivetskiy, S. A.; McLean, M. A.; Morizumi, T.; Huang, C.; Tesmer, J. J. G.; Ernst, O. P.; Sligar, S. G.; Gurevich, V. V. Monomeric Rhodopsin Is Sufficient for Normal Rhodopsin Kinase (GRK1) Phosphorylation and Arrestin-1 Binding. *J. Biol. Chem.* **2011**, *286*, 1420−1428.
(23) Boldog, T.; Grimme, S.; Li, M.; Sligar, S. G.; Hazelbauer, G. L. Nanodiscs Separate Chemoreceptor Oligomeric States and Reveal Their Signaling Properties. *Proc. Natl. Acad. Sci. U. S. A.* **2006**, *103*, 11509−11514.
(24) Bayburt, T. H.; Sligar, S. G. Single-Molecule Height Measurements on Microsomal Cytochrome P450 in Nanometer-Scale Phospholipid Bilayer Disks. *Proc. Natl. Acad. Sci. U. S. A.* **2002**, *99*, 6725−6730.
(25) Bayburt, T. H.; Carlson, J. W.; Sligar, S. G. Single Molecule Height Measurements on a Membrane Protein in Nanometer-Scale Phospholipid Bilayer Disks. *Langmuir* **2000**, *16*, 5993−5997.
(26) Bayburt, T. H.; Grinkova, Y. V.; Sligar, S. G. Assembly of Single Bacteriorhodopsin Trimers in Bilayer Nanodiscs. *Arch. Biochem. Biophys.* **2006**, *450*, 215−222.
(27) Bayburt, T. H.; Sligar, S. G. Self-Assembly of Single Integral Membrane Proteins into Soluble Nanoscale Phospholipid Bilayers. *Protein Sci.* **2003**, *12*, 2476−2481.
(28) Gao, T.; Petrlova, J.; He, W.; Huser, T.; Kudlick, W.; Voss, J.; Coleman, M. A. Characterization of De Novo Synthesized GPCRs Supported in Nanolipoprotein Discs. *PLoS One* **2012**, *7*, e44911.
(29) Inagaki, S.; Ghirlando, R.; White, J. F.; Gvozdenovic-Jeremic, J.; Northup, J. K.; Grisshammer, R. Modulation of the Interaction between Neurotensin Receptor NTS1 and Gq Protein by Lipid. *J. Mol. Biol.* **2012**, *417*, 95−111.
(30) Ishida, H.; Garcia-Herrero, A.; Vogel, H. J. The Periplasmic Domain of Escherichia Coli Outer Membrane Protein A Can Undergo a Localized Temperature Dependent Structural Transition. *Biochim. Biophys. Acta, Biomembr.* **2014**, *1838*, 3014−3024.
(31) Hagn, F.; Etzkorn, M.; Raschle, T.; Wagner, G. Optimized Phospholipid Bilayer Nanodiscs Facilitate High-Resolution Structure Determination of Membrane Proteins. *J. Am. Chem. Soc.* **2013**, *135*, 1919−1925.
(32) Shih, A. Y.; Freddolino, P. L.; Sligar, S. G.; Schulten, K. Disassembly of Nanodiscs with Cholate. *Nano Lett.* **2007**, *7*, 1692−1696.
(33) Marty, M. T.; Zhang, H.; Cui, W.; Blankenship, R. E.; Gross, M. L.; Sligar, S. G. Native Mass Spectrometry Characterization of Intact Nanodisc Lipoprotein Complexes. *Anal. Chem.* **2012**, *84*, 8957−8960.
(34) Wadsäter, M.; Maric, S.; Simonsen, J. B.; Mortensen, K.; Cardenas, M. The Effect of Using Binary Mixtures of Zwitterionic and Charged Lipids on Nanodisc Formation and Stability. *Soft Matter* **2013**, *9*, 2329.
(35) Denisov, I. G.; McLean, M. a; Shaw, A. W.; Grinkova, Y. V.; Sligar, S. G. Thermotropic Phase Transition in Soluble Nanoscale Lipid Bilayers. *J. Phys. Chem. B* **2005**, *109*, 15580−15588.
(36) Mörs, K.; Roos, C.; Scholz, F.; Wachtveitl, J.; Dötsch, V.; Bernhard, F.; Glaubitz, C. Modified Lipid and Protein Dynamics in Nanodiscs. *Biochim. Biophys. Acta, Biomembr.* **2013**, *1828*, 1222−1229.
(37) Morgan, C. R.; Hebling, C. M.; Rand, K. D.; Stafford, D. W.; Jorgenson, J. W.; Engen, J. R. Conformational Transitions in the Membrane Scaffold Protein of Phospholipid Bilayer Nanodiscs. *Mol. Cell. Proteomics* **2011**, *10*, M111.010876.
(38) Klon, A. E.; Segrest, J. P.; Harvey, S. C. Molecular Dynamics Simulations on Discoidal HDL Particles Suggest a Mechanism for Rotation in the Apo A-I Belt Model. *J. Mol. Biol.* **2002**, *324*, 703−721.
(39) Catte, A.; Patterson, J. C.; Jones, M. K.; Jerome, W. G.; Bashtovyy, D.; Su, Z.; Gu, F.; Chen, J.; Aliste, M. P.; Harvey, S. C.; Li, L.; Weinstein, G.; Segrest, J. P. Novel Changes in Discoidal High Density Lipoprotein Morphology: A Molecular Dynamics Study. *Biophys. J.* **2006**, *90*, 4345−4360.
(40) Segrest, J. P.; Jones, M. K.; Catte, A.; Thirumuruganandham, S. P. Validation of Previous Computer Models and MD Simulations of Discoidal HDL by a Recent Crystal Structure of apoA-I. *J. Lipid Res.* **2012**, *53*, 1851−1863.
(41) Wako, H.; Endo, S. Ligand-Induced Conformational Change of a Protein Reproduced by a Linear Combination of Displacement Vectors Obtained from Normal Mode Analysis. *Biophys. Chem.* **2011**, *159*, 257−266.
(42) Shih, A. Y.; Sligar, S. G.; Schulten, K. Molecular Models Need to Be Tested: The Case of a Solar Flares Discoidal HDL Model. *Biophys. J.* **2008**, *94*, L87−L89.
(43) Wassenaar, T. A.; Pluhackova, K.; Böckmann, R. A.; Marrink, S. J.; Tieleman, D. P. Going Backward: A Flexible Geometric Approach to Reverse Transformation from Coarse Grained to Atomistic Models. *J. Chem. Theory Comput.* **2013**, *10*, 676−690.
(44) Luecke, H.; Schobert, B.; Richter, H.-T.; Cartailler, J.-P.; Lanyi, J. K. Structure of Bacteriorhodopsin at 1.55 Å Resolution 1. *J. Mol. Biol.* **1999**, *291*, 899−911.
(45) Deng, D.; Xu, C.; Sun, P.; Wu, J.; Yan, C.; Hu, M.; Yan, N. Crystal Structure of the Human Glucose Transporter GLUT1. *Nature* **2014**, *510*, 121−125.

DOI: 10.1021/acs.jctc.5b00668
J. Chem. Theory Comput. 2015, 11, 4923−4932

(46) Vogt, J.; Schulz, G. E. The Structure of the Outer Membrane Protein OmpX from Escherichia Coli Reveals Possible Mechanisms of Virulence. *Structure* **1999**, *7*, 1301−1309.
(47) Van der Spoel, D.; Lindahl, E.; Hess, B.; Groenhof, G.; Mark, A. E.; Berendsen, H. J. C. GROMACS: Fast, Flexible, and Free. *J. Comput. Chem.* **2005**, *26*, 1701−1718.
(48) van der Spoel, D.; Lindahl, E.; Hess, B.; van Buuren, A. R.; Apol, E.; Meulenhoff, P. J.; Tieleman, D. P.; Sijbers, A. L. T. M.; Feenstra, K. A.; van Drunen, R.; Berendsen, H. J. C. *Gromacs User Manual*, version 4.5.4; Uppsala University: Uppsala, Sweden, 2010.
(49) Rozmanov, D. *Bio.B-Gen*. http://sourceforge.net/projects/biobgen/.
(50) Marrink, S. J.; de Vries, A. H.; Mark, A. E. Coarse Grained Model for Semiquantitative Lipid Simulations. *J. Phys. Chem. B* **2004**, *108*, 750−760.
(51) Marrink, S. J.; Risselada, J. H.; Yefimov, S.; Tieleman, P. D.; de Vries, A. H. The MARTINI Force Field: Coarse Grained Model for Biomolecular Simulations. *J. Phys. Chem. B* **2007**, *111*, 7812−7824.
(52) Monticelli, L.; Kandasamy, S. K.; Periole, X.; Larson, R. G.; Tieleman, P. D.; Marrink, S.-J. The MARTINI Coarse-Grained Force Field: Extension to Proteins. *J. Chem. Theory Comput.* **2008**, *4*, 819−834.
(53) De Jong, D. H.; Singh, G.; Bennett, D. W. F.; Arnarez, C.; Wassenaar, T. A.; Schafer, L. V.; Periole, X.; Tieleman, P. D.; Marrink, S. J.; East, M.; Melville, D.; Lee, A. G. Improved Parameters For The Martini Coarse-Grained Protein Force Field. *J. Chem. Theory Comput.* **2013**, *9*, 687−697.
(54) Ingólfsson, H. I.; Melo, M. N.; van Eerden, F. J.; Arnarez, C.; Lopez, C. A.; Wassenaar, T. A.; Periole, X.; de Vries, A. H.; Tieleman, D. P.; Marrink, S. J. Lipid Organization of the Plasma Membrane. *J. Am. Chem. Soc.* **2014**, *136*, 14554−14559.
(55) Periole, X.; Cavalli, M.; Marrink, S.-J.; Ceruso, M. A. Combining an Elastic Network With a Coarse-Grained Molecular Force Field: Structure, Dynamics, and Intermolecular Recognition. *J. Chem. Theory Comput.* **2009**, *5*, 2531−2543.
(56) Berendsen, H. J. C.; Postma, J. P. M.; van Gunsteren, W. F.; Dinola, A.; Haak, J. R. Molecular-Dynamics with Coupling to an External Bath. *J. Chem. Phys.* **1984**, *81*, 3684−3690.
(57) Parrinello, M.; Rahman, A. Polymorphic Transitions in Single Crystals: A New Molecular Dynamics Method. *J. Appl. Phys.* **1981**, *52*, 7182−7190.
(58) Bussi, G.; Donadio, D.; Parrinello, M. Canonical Sampling Through Velocity Rescaling. *J. Chem. Phys.* **2007**, *126*, 014101.
(59) Lindorff-Larsen, K.; Piana, S.; Palmo, K.; Maragakis, P.; Klepeis, J. L.; Dror, R. O.; shaw, D. E. Improved Side-Chain Torsion Potentials for the Amber ff99SB Protein Force Field. *Proteins: Struct., Funct., Genet.* **2010**, *78*, 1950−1958.
(60) Jämbeck, J. P. M.; Lyubartsev, A. P. Another Piece of the Membrane Puzzle: Extending Slipids Further. *J. Chem. Theory Comput.* **2013**, *9*, 774−784.
(61) Jämbeck, J. P. M.; Lyubartsev, A. P. An Extension and Further Validation of an All-Atomistic Force Field for Biological Membranes. *J. Chem. Theory Comput.* **2012**, *8*, 2938−2948.
(62) Jämbeck, J. P. M.; Lyubartsev, A. P. Derivation and Systematic Validation of a Refined All-Atom Force Field for Phosphatidylcholine Lipids. *J. Phys. Chem. B* **2012**, *116*, 3164−3179.
(63) Domański, J.; Stansfeld, P.; Sansom, M. P.; Beckstein, O. Lipidbook: A Public Repository for Force-Field Parameters Used in Membrane Simulations. *J. Membr. Biol.* **2010**, *236*, 255−258.
(64) Jorgensen, W. L.; Chandrasekhar, J.; Madura, J. D.; Impey, R. W.; Klein, M. L. Comparison of Simple Potential Functions for Simulating Liquid Water. *J. Chem. Phys.* **1983**, *79*, 926−935.
(65) Darden, T.; York, D.; Pedersen, L. PARTICLE MESH EWALD - AN N.LOG(N) METHOD FOR EWALD SUMS IN LARGE SYSTEMS. *J. Chem. Phys.* **1993**, *98*, 10089−10092.
(66) Humphrey, W.; Dalke, A.; Schulten, K. VMD: Visual Molecular Dynamics. *J. Mol. Graphics* **1996**, *14*, 33.
(67) Castillo, N.; Monticelli, L.; Barnoud, J.; Tieleman, D. P. Free Energy of WALP23 Dimer Association in DMPC, DPPC, and DOPC Bilayers. *Chem. Phys. Lipids* **2013**, *169*, 95−105.
(68) Klon, A. E.; Jones, M. K.; Segrest, J. P.; Harvey, S. C. Molecular Belt Models for the Apolipoprotein A-I Paris and Milano Mutations. *Biophys. J.* **2000**, *79*, 1679−1685.
(69) Ritchie, T. K.; Grinkova, Y. V.; Bayburt, T. H.; Denisov, I. G.; Zolnerciks, J. K.; Atkins, W. M.; Sligar, S. G. Reconstitution of Membrane Proteins in Phospholipid Bilayer Nanodiscs. *Methods Enzymol.* **2009**, *464*, 211−231.
(70) Scott, K. A.; Bond, J.; Ivetac, A.; Chetwynd, A. P.; Khalid, S.; Sansom, M. S. P. Coarse-Grained MD Simulations of Membrane Protein-Bilayer Self-Assembly. *Structure* **2008**, *16*, 621−630.
(71) Bond, P. J.; Sansom, M. S. P. Bilayer Deformation by the Kv Channel Voltage Sensor Domain Revealed by Self-Assembly Simulations. *Proc. Natl. Acad. Sci. U. S. A.* **2007**, *104*, 2631−2636.
(72) Hall, B. A.; Chetwynd, A. P.; Sansom, M. S. P. Exploring Peptide-Membrane Interactions with Coarse-Grained MD Simulations. *Biophys. J.* **2011**, *100*, 1940−1948.
(73) Psachoulia, E.; Marshall, D. P.; Sansom, M. S. P. Molecular Dynamics Simulations of the Dimerization of Transmembrane Alpha-Helices. *Acc. Chem. Res.* **2010**, *43*, 388−396.
(74) König, B.; Dietrich, U.; Klose, G. Hydration and Structural Properties of Mixed Lipid/Surfactant Model Membranes. *Langmuir* **1997**, *13*, 525−532.
(75) Kucerka, N.; Tristram-Nagle, S.; Nagle, J. F. Structure of Fully Hydrated Fluid Phase Lipid Bilayers with Monounsaturated Chains. *J. Membr. Biol.* **2005**, *208*, 193−202.
(76) Kučerka, N.; Liu, Y.; Chu, N.; Petrache, H. I.; Tristram-Nagle, S.; Nagle, J. F. Structure of Fully Hydrated Fluid Phase DMPC and DLPC Lipid Bilayers Using X-Ray Scattering from Oriented Multilamellar Arrays and from Unilamellar Vesicles. *Biophys. J.* **2005**, *88*, 2626−2637.
(77) Anton, N.; Saulnier, P.; Boury, F.; Foussard, F.; Benoit, J.-P.; Proust, J. E. The Influence of Headgroup Structure and Fatty Acyl Chain Saturation of Phospholipids on Monolayer Behavior: A Comparative Rheological Study. *Chem. Phys. Lipids* **2007**, *150*, 167−175.
(78) Ackerman, D. G.; Feigenson, G. W. Multiscale Modeling of Four-Component Lipid Mixtures: Domain Composition, Size, Alignment, and Properties of the Phase Interface. *J. Phys. Chem. B* **2015**, *119*, 4240−4250.
(79) Pluhackova, K.; Wassenaar, T. A.; Kirsch, S.; Böckmann, R. A. Spontaneous Adsorption of Coiled-Coil Model Peptides K and E to a Mixed Lipid Bilayer. *J. Phys. Chem. B* **2015**, *119*, 4396−408.
(80) Hinsen, K.; Vaitinadapoule, A.; Ostuni, M. A.; Etchebest, C.; Lacapere, J.-J. Construction and Validation of an Atomic Model for Bacterial TSPO from Electron Microscopy Density, Evolutionary Constraints, and Biochemical and Biophysical Data. *Biochim. Biophys. Acta, Biomembr.* **2015**, *1848*, 568−580.
(81) Konijnenberg, A.; Yilmaz, D.; Ingólfsson, H. I.; Dimitrova, A.; Marrink, S. J.; Li, Z.; Vénien-Bryan, C.; Sobott, F.; Koçer, A. Global Structural Changes of an Ion Channel during Its Gating Are Followed by Ion Mobility Mass Spectrometry. *Proc. Natl. Acad. Sci. U. S. A.* **2014**, *111*, 17170−17175.
(82) Siuda, I.; Thøgersen, L. Conformational Flexibility of the Leucine Binding Protein Examined by Protein Domain Coarse-Grained Molecular Dynamics. *J. Mol. Model.* **2013**, *19*, 4931−4945.
(83) Skar-Gislinge, N.; Simonsen, J. B.; Mortensen, K.; Feidenhans'l, R.; Sligar, S. G.; Møller, B. L.; Bjørnholm, T.; Arleth, L. Elliptical Structure of Phospholipid Bilayer Nanodiscs Encapsulated by Scaffold Proteins: Casting the Roles of the Lipids and the Protein. *J. Am. Chem. Soc.* **2010**, *132* (39), 13713−13722.
(84) Castillo, N.; Monticelli, L.; Barnoud, J.; Tieleman, D. P. Free energy of WALP23 dimer association in DMPC, DPPC and DOPC bilayers. *Chem. Phys. Lipids* **2013**, *169*, 95−105.

DOI: 10.1021/acs.jctc.5b00668
J. Chem. Theory Comput. 2015, 11, 4923−4932